



HAL
open science

Electric Field Distribution in HVDC Cable Joint in Non-Stationary Conditions

Thi Thu Nga Vu, G. Teyssedre, Séverine Le Roy

► **To cite this version:**

Thi Thu Nga Vu, G. Teyssedre, Séverine Le Roy. Electric Field Distribution in HVDC Cable Joint in Non-Stationary Conditions. *Energies*, 2021, 14 (5401), pp.17. 10.3390/en14175401 . hal-03382516

HAL Id: hal-03382516

<https://hal.science/hal-03382516>

Submitted on 16 Nov 2021

HAL is a multi-disciplinary open access archive for the deposit and dissemination of scientific research documents, whether they are published or not. The documents may come from teaching and research institutions in France or abroad, or from public or private research centers.

L'archive ouverte pluridisciplinaire **HAL**, est destinée au dépôt et à la diffusion de documents scientifiques de niveau recherche, publiés ou non, émanant des établissements d'enseignement et de recherche français ou étrangers, des laboratoires publics ou privés.

2 **Electric Field Distribution in HVDC Cable Joint in** 3 **Non-Stationary Conditions**

4 **Thi Thu Nga Vu^{1,*}, Gilbert Teyssedre^{2,*} and Séverine Le Roy^{2,*}**

5 ¹ Electric Power University, Hanoi, Vietnam.

6 ² Laplace, University of Toulouse and CNRS, Toulouse, France.

7 * Correspondence: ngavtt@epu.edu.vn (T.T.N.V.); gilbert.teyssedre@laplace.univ-
8 tlse.fr (G.T.); severine.leroy@laplace.univ-tlse.fr (S.L.R.)

9 **Abstract:** Accessories such as joints and terminations represent weak points in HVDC cable systems. Indeed, the
10 DC field distribution is intimately dependent on the thermal conditions of the accessory and on material proper-
11 ties. Moreover, there is no available method to probe charge distribution in those conditions. In this work, the
12 field distribution in non-stationary conditions, both thermally and electrically, is computed considering cross-
13 linked polyethylene (XLPE) as cable insulation and different insulating materials (silicone, rubber, XLPE) for a
14 200kV joint assembled in a same geometry. In the conditions used, i.e. temperatures up to 70°C, and with the
15 material properties considered, the dielectric time constant appears of the same order or even longer than the
16 thermal one and is of several hours. It means that both physical phenomena need to be considered for modelling
17 the electric field distribution. Both the radial and the tangential field distributions are analysed, and focus is given
18 on the field distribution under the stress cone on the ground side and near the central deflector on the high voltage
19 side of the joint. We show that the position of the maximum field varies in time in a way that is not easy to
20 anticipate. Under the cone, the smallest tangential field is obtained with the joint insulating material having the
21 highest electrical conductivity. It results from a shift of the field towards the cable insulation in which the geo-
22 metrical features produce less axial component of the field. At the level of the central deflector, it is clear that the
23 tangential field is higher when the mismatch between the conductivity of the two insulations is larger. In addition,
24 the field grows as a function of time under stress. The work points to the need of precise data on materials con-
25 ductivity and to the need of probing field distribution in 3D.

26 **Keywords:** HVDC cable system; accessories; space charge; field distribution

27 **1. Introduction**

28 Accessories may represent a weak point in HVDC cable links, especially when going to ever-higher
29 voltages where the feedback on in-service behaviour is lacking [1, 2]. Compared to bulk cables where
30 many research works are carried out, both experimentally and in modelling, for assessing insulation
31 endurance, anticipating field distribution in accessories is more difficult to tackle. Especially, methods
32 for probing charge and field distributions in localized areas are lacking and the fact that different
33 insulating materials coexist brings further difficulty. For this reason, thermal and electrical modelling
34 is necessary. Various degrees of sophistication can be achieved for DC field modelling of insulations
35 [3], ranging from bipolar charge transport model with identification of generation, transport and trap-
36 ping processes of charges, to macroscopic models based on conductivity expression. Resorting to mac-
37 roscopic modelling, i.e. based on field and temperature dependencies of conductivity and/or permit-
38 tivity, the numerical resolution of the problem is not a real difficulty. However, it must be based on
39 reliable experimental data characterizing the materials, especially conductivity, and on the exploration
40 of different practical combinations of thermal/electrical stresses that may be encountered.

41 In this contribution, we report mainly on the modelling of the electric field distribution in unsteady
42 situations from the electrical and thermal point of view in cable accessories comprising an association
43 of insulators of different nature in a specific geometry. In many situations, simulations have been car-
44 ried out on admittedly complex objects, but in a stationary situation [4]. However, one must wonder

45 about the redistribution of the electric field in the case where the transmitted power suddenly in-
46 creases, implying to have a thermal transient in the accessory, and also to have an idea of the thermal
47 equilibrium time of the system. The transient in electrical stress obviously involves the passage from
48 a capacitive distribution to a resistive distribution of the electric field after energizing the cable and
49 joint, with an 'electric' time constant depending on the temperature. It is also important to estimate
50 the maximum field values that can be obtained during operation, particularly in the case of polarity
51 inversion of the applied voltage, for inverting the power flow using Line-commutated converters, LCC
52 [5]. Modelling may help anticipating the 'hot spots' of electrical stress during operations on the system,
53 such as these polarity reversals or temperature variations linked to fluctuations in the transmitted
54 power. In addition, 'type' and pre-qualification tests at $1.85 \times U_0$ and $1.45 \times U_0$, where U_0 is the nom-
55 inal service voltage, also involving variations in the current over several hours as well as polarity
56 reversals or pulse tests, must be taken into account in the design [6, 7].

57 As stated previously, accessories represent weak points of the transmission system. Cable joints are
58 mainly of two types for cables with extruded insulation [1], generally made of cross-linked polyeth-
59 ylene (XLPE). The 'factory' joints apply mainly to submarine cables, and are processed at the time of
60 extrusion, for example for jointing two cables of several tens of km each, for the purpose of production
61 lines maintenance. They are compact and reform the cable almost identically. The materials and pro-
62 cesses used are the same as those of the cable insulation. Prefabricated - or pre-moulded joints, on the
63 other hand, are made using a material different from that of the cable insulation. They are generally
64 made of elastomers as silicone rubber (SiR) or ethylene-propylene-diene monomer terpolymer
65 (EPDM). They are manufactured during the laying of cables, in particular at the junction of cable sec-
66 tions of limited length for buried cables for logistical reasons. Rebuilding the insulation and all cable
67 components takes more space than for factory junctions. On part of the joint, the extruded insulation
68 and material joint coexist.

69 It is recognized that the dielectric/dielectric interface represents a threat for the accessory reliability
70 and the tangential field can be a driving mode for failure [1, 8, 9, 10]. Whereas the behaviour of the
71 radial field distribution in a bilayer dielectric can be reasonably anticipated based on the conductivity
72 behaviour, the tangential component is more difficult to tackle, especially the respective role of geom-
73 etry and thermal stress.

74 In this work, based on a conductivity law established from experiments on typical materials that are
75 XLPE, SiR, and EPDM, the field distribution in a 200 kV cable joint is computed. Polarity reversal of
76 the DC stress after long charging time is considered, as well as different thermal conditions: isothermal
77 at 30 °C and non-stationary thermal gradient when energizing the cable. The tangential and radial
78 electric fields are computed in these transient electrical and thermal conditions. To evaluate how far
79 the nature of material imparts the field distribution, the case of a joint fully made of XLPE, as could
80 be the case for factory joints [1], is considered. We also modelled the association of silicone rubber
81 (SiR) with XLPE.

82 **2. Joint Characteristics and Model**

83 *2.1. Geometry*

84 The object of the present study is a 200 kV, 1 kA HVDC joint with general design and geometry as
85 given in Figure 1 [11]. The cable insulation is made of XLPE. The pre-moulded sleeve is initially made
86 of EPDM. The nature of this material and corresponding properties will be changed in the modelling
87 to investigate the impact on the field distribution.

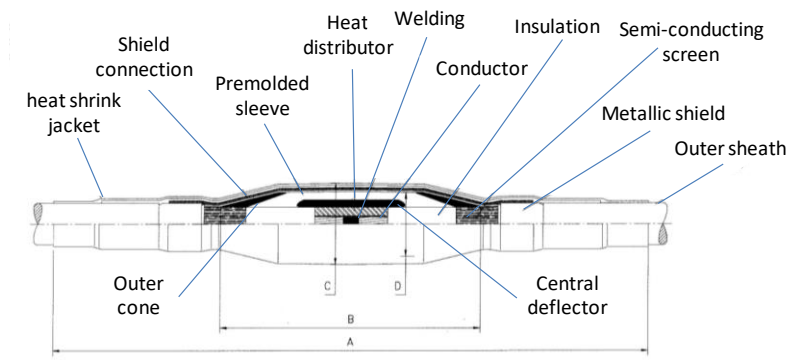


Figure 1. Scheme of the modelled joint with main approximate dimensions: length 800 mm, conductor radius 22.8 mm, insulation thickness 20 mm in the cable and 70 mm in the joint.

Field distribution cones are present at both ends of the joint and a central deflector covers the welding. The cones and the deflector are made of semiconductor material (semicon), i.e. a carbon black charged polymer. The semiconducting layer is also present on the conductor. In the model described here, the outer layer, which normally contains shielding layers, is simplified by using a 5 mm thick semicon layer ensuring electrical continuity and providing thermal resistance at the surface of the joint. The field distribution in the insulation layers comprised between the outer cone and the central deflector is investigated.

2.2. Materials properties

The data on conductivity versus field and temperature of XLPE and EPDM materials are detailed elsewhere [12, 13]. The following equation has been parameterized using experimental data on current obtained as a function of electric field on plane samples.

$$\sigma(T, E) = A \cdot \exp\left(\frac{-E_a}{k_B T}\right) \cdot \sinh(\beta(T) \cdot E) \cdot E^\alpha \quad (1)$$

where the pre-exponential factor A , activation energy E_a , field coefficients $\beta(T)=aT+b$ and α are given in Table 1 [13] and k_B is the Boltzmann's constant. The parameters are listed for conductivity given in S/m, the field in V/m, the temperature in K.

Table 1. Parameters of the conductivity equation used for XLPE and EPDM materials.

	XLPE	EPDM
A (S.I.)	0.8	97
E_a (eV)	1.0	0.44
a (m/V/K)	0 (T < 313 K); -1.3 × 10 ⁻⁹ (T ≥ 313 K)	4.8 × 10 ⁻¹⁰
b (m/V)	1.38 × 10 ⁻⁷ (T < 313 K); 5.45 × 10 ⁻⁷ (T ≥ 313 K)	-5.1 × 10 ⁻⁸
α	0.15	-1.42

For the silicone rubber, the expression of conductivity given by Baferani *et al* [14] was adopted:

$$\sigma(T, E) = A \cdot \exp(\gamma T) \cdot \exp(\beta E) \quad (2)$$

with $A = 2.9 \times 10^{-17}$ S/m, the temperature coefficient is $\gamma = 0.019$ K⁻¹ and $\beta = 4.1 \times 10^{-16}$ mm/kV.

Figure 2 shows a comparison of conductivity as a function of the electric field for the different materials at different temperatures. The behaviour for XLPE is in line with previous report [15]. For EPDM, a decrease of the conductivity with field appears, which may appear not common. This behaviour was discussed in a previous work [12] and it was suggested that some form of ionic processes might be at play in the sub-linear behaviour, as may happen in insulating liquids. Not many reports on DC conductivity measurements using reasonable charging time are available in the literature for EPDM. In a recent work, Z.Y. Li *et al* [16] reported on quasi field-independent conductivity of EPDM for fields up to 10 to 20kV/mm that contrasted with the strong field dependence of conductivity of XLPE. Besides, EPDM is a complex material and its behaviour may change with compounding: D. Li *et al* [17] found power law relation between conductivity and field with an exponent n in the range from 0.2 to 0.9 depending on EPDM grade (with using only 1min charging time!). The conductivity of SiR exhibits very weak field dependence and relatively mild temperature dependence. Another expression proposed by Qin *et al* [18] follows the same trend.

Comparing XLPE and EPDM, the conductivity is sometimes higher in one material or the other, depending on the field and temperature conditions, which will result in a transfer of the DC field in one or the other of the materials according to these same conditions

The other physical quantities used in the model are reported in Table 2. The heat input by the Joule effect in the copper conductor takes into account a reference resistivity of $1.7 \times 10^{-8} \Omega \cdot m$ for copper at 20 °C and a temperature coefficient for the resistivity of $3.9 \times 10^{-3} K^{-1}$.

Table 2. Material parameters used in the model.

	XLPE	EPDM	SiR	Semicon
Relative permittivity ϵ_r	2.30	2.90	3.50	2.30
Thermal cond. λ (W/m/K)	0.38	0.30	0.20	0.34
Specific heat c_p (J/g/K)	1.90	0.73	2.25	1.90
Electrical cond. σ (S/m)	cf. Eq. (1)		cf. Eq. (2)	6.0×10^3

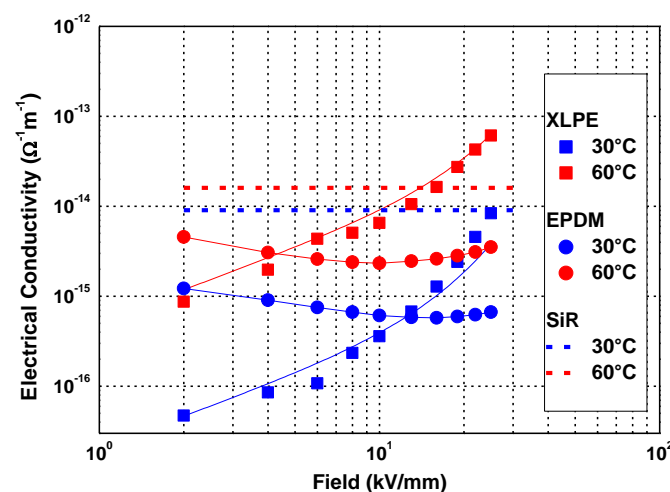


Figure 2. Field dependence of the electrical conductivity of XLPE, EPDM and SiR at 30 and 60 °C.

2.3. Thermal-electrical model

The resolution of the field distribution was carried out using the Comsol® tool using the thermal and electrical modules. Owing to the cylindrical symmetry of cable joints, the considered geometries are built up as 2D axisymmetric models. The general equations to be solved are the following:

-Maxwell equation reduced to the DC case [7]:

$$-\nabla \frac{\partial(\epsilon \nabla V)}{\partial t} - \nabla(\sigma \nabla V) = 0 \quad (3)$$

138 which becomes in local form and in continuous medium, the continuity equation:

$$\frac{\partial \rho}{\partial t} + \nabla J = 0 \quad (4)$$

139 -Equation of thermal dynamics:

$$\rho_m c_p \frac{\partial T}{\partial t} - \nabla(\lambda \nabla T) = Q \quad (5)$$

140 where ρ_m is the density, c_p the specific heat, λ the thermal conductivity, Q the heat source.

141 The electric stress is applied to the conductor, using a nominal voltage of ± 200 kV. The electric field
 142 distribution is calculated under unsteady conditions with 24 h energizing, short-circuiting, and during
 143 polarity reversals. Switching from one polarity to another is done with an intermediate short-circuit
 144 of 3 min. A duration of 24 h was chosen to approach a stationary situation both from the thermal and
 145 electrical point of view. Indeed, in a previous work on the association of EPDM and XLPE, the dielec-
 146 tric time constant was of the order of 24h at 20°C [19]. As the minimum temperature is 30°C in the
 147 present work, it was considered that 24h was enough for reaching the steady state. For the thermal
 148 response, the first simulations showed that 24h was actually enough for obtaining a steady state (see
 149 below).

150 Thermal modelling is carried out by considering a heat input by the Joule effect in the conductor and
 151 external losses by convection phenomena in the air. The considered conductor cross section is 50 mm².
 152 The power dissipated in the conductor is of the order of 350 W/m under 1 kA at 30 °C. Heat exchange
 153 with the surrounding environment is assumed to occur by natural convection:

$$q_c = h(T_s - T_{amb}) \quad (6)$$

154 where h represents the convective transfer coefficient, linked to the Nusselt number (h of the order of
 155 5 W/m²/K taking into account the geometry of the cable is rigorously determined in the resolution
 156 software). T_s and T_{amb} are the joint surface temperature and the ambient temperature, respectively.
 157 The heat flux exchanged by radiation (which remains low under our thermal conditions) is also taken
 158 into account by considering a surface emissivity coefficient of 0.8.

159 3. Results

160 Figure 3 shows the dimensions of the modelled object, of external radius 92 mm. For the representa-
 161 tion of the radial distribution of the field in the form of profiles, an axial position at $z = 800$ mm was
 162 chosen, such to be halfway between the deflector cone and the internal semiconductor. The axial dis-
 163 tribution of the field is taken at the interface between the XLPE insulation and the joint material as this
 164 region is critical and constitutes a weak point of the joint.

165 The applied stresses are those previously mentioned (± 200 kV). We have considered three thermal
 166 conditions: a homogeneous temperature at $T = 30$ °C, a stationary condition with a thermal gradient
 167 due to the injection of a current of 1 kA in the conductor, and an unsteady condition both from an
 168 electrical and thermal point of view, keeping the same current flowing in the conductor and consid-
 169 ering a homogeneous initial temperature of 30 °C. The limit conditions are a constant potential applied
 170 to the conductor and welding, and reference potential to the outer surface of the joint.

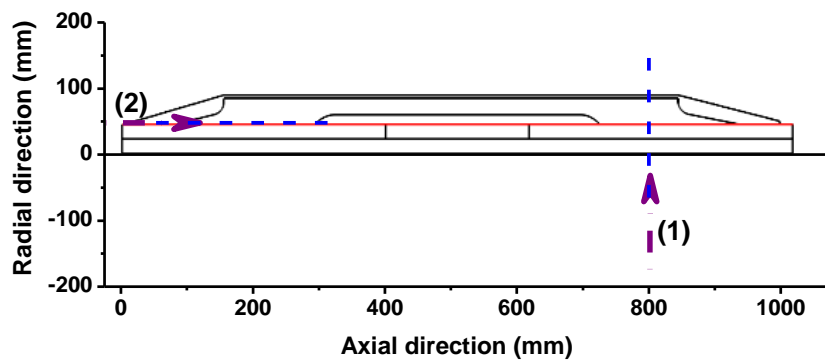


Figure 3. Dimensions of the joint and positions of the simulated field profiles indicated by arrows: (1) Radially at a position $z = 800$ mm at mid-distance between the outer cone and central deflector; (2) axially: along the interface between the two insulators.

3.1. Thermal simulation

The thermal modelling of the XLPE/EPDM joint was carried out assuming that the joint was initially at an isothermal temperature of 30°C . At $t = 0$ s, a current of 1 kA is imposed on the conductor, which has the effect of slowly heating the joint and producing a thermal gradient within the insulation. The final temperature gradient is of the order of 40°C , with a temperature maximum situated between the end of the internal deflector and the end of the joint. It corresponds to the region where the insulation is the thickest, due to the low thermal conductivity. Figure 4a) shows the temperature distribution in the joint after 3 min and 8 h of heating, while Figure 4b) shows the change in temperature as a function of the heating time for a cut at $z = 800$ mm. The temperature profile resulting from a resolution in stationary condition is also represented. It can be seen that several hours are necessary to reach a steady state. Even after 16 h, the thermal equilibrium is not completely reached. The interface between the two insulators, XLPE and EPDM in this case, is not very marked because the thermal conductivities are close, see Table 2.

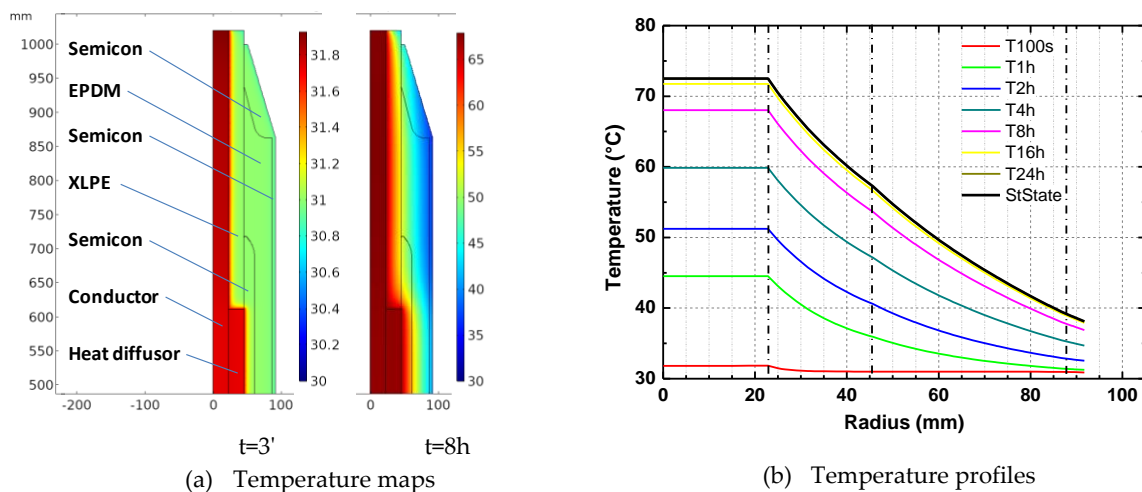


Figure 4. a) Temperature distribution maps in the joint with XLPE/EPDM insulations at different times after applying the current of 1 kA in the conductor; b) Radial temperature distribution at different times and stationary solution, taken at $z = 800$ mm. Vertical lines indicate the boundaries of the insulators.

3.2. Electric Field Distribution

Examples of electric field distributions as a function of time under applied voltage and polarity reversals, obtained for the joint with EPDM insulation on XLPE-insulated cable are shown in Figure 5. The voltage is considered applied when the current is applied to the conductor. One can notice that over

time, a field strengthening effect occurs, particularly under the field distributing cone. This is partly because the regions of reinforced geometric field are also those with the lowest temperature: the increase in temperature in the centre of the joint causes an increase in electrical conductivity and shifts the field to colder areas. When the voltage is set to zero, a residual field of the order of 6 kV/mm is present. After polarity reversal, the field is clearly increased locally, with a maximum value of the order of 18 kV/mm. The accumulated charge during previous charging requires a relatively long time to be dissipated and redistributed. The objective is to follow the evolution of the position of the field reinforcement points over time.

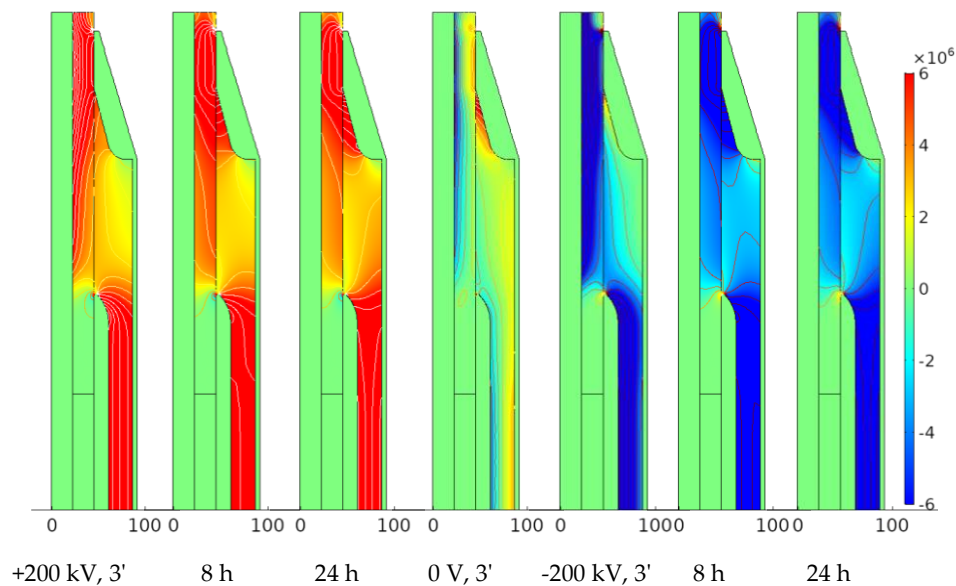


Figure 5. Some examples of radial field maps in the joint after application of a current of 1 kA and voltage of +200 kV ($t = 0$) switched to -200 kV after 24 h.

In order to dissociate the thermal effects from the nonlinear electrical conduction effects on the field distribution, we considered the field distributions obtained in a transient manner, under a voltage of 200 kV applied for 24 hours, followed by a polarity reversal and again by a stressing under -200 kV for 24 h. This protocol was applied for 3 different thermal conditions: an isotherm at 30°C, a stationary thermal gradient condition (pre-set current of 1 kA), and finally the case illustrated above where the electrical and thermal stresses are applied simultaneously. Details of the field distribution evolution are presented considering the radial and tangential components.

3.2.1. Distribution of the radial component of the electric field

The results obtained for the radial distribution of the field at the position $z = 800$ mm are shown in Figure 6 for XLPE/EPDM joint. As will be shown in section 3.2.2, the axial component of the field is almost zero at this position. The field distribution under isothermal conditions (Figure 6a) is clearly distinguished from the other cases. At 100 s, i.e. short after voltage application, the field is capacitively distributed. Hence, $E_{XLPE} > E_{EPDM}$ due to the lower dielectric permittivity in XLPE. As expected, this initial field profile is independent from the thermal conditions, since no temperature dependence of the dielectric permittivity was introduced in the model.

For the isothermal case at 30 °C, the field gradually evolves in time with further field reinforcement in XLPE, without any pronounced change in the general shape. This evolution corresponds to two phenomena: on the one hand, it is the consequence of a resistivity at 30 °C of XLPE greater than that of EPDM, for fields < 10 kV/mm, cf. Figure 2. The other feature is that the field strengths remain moderate (< 10 kV/mm) so that the nonlinear phenomena, tending to a homogenization of the field over time, are barely perceptible in the two materials.

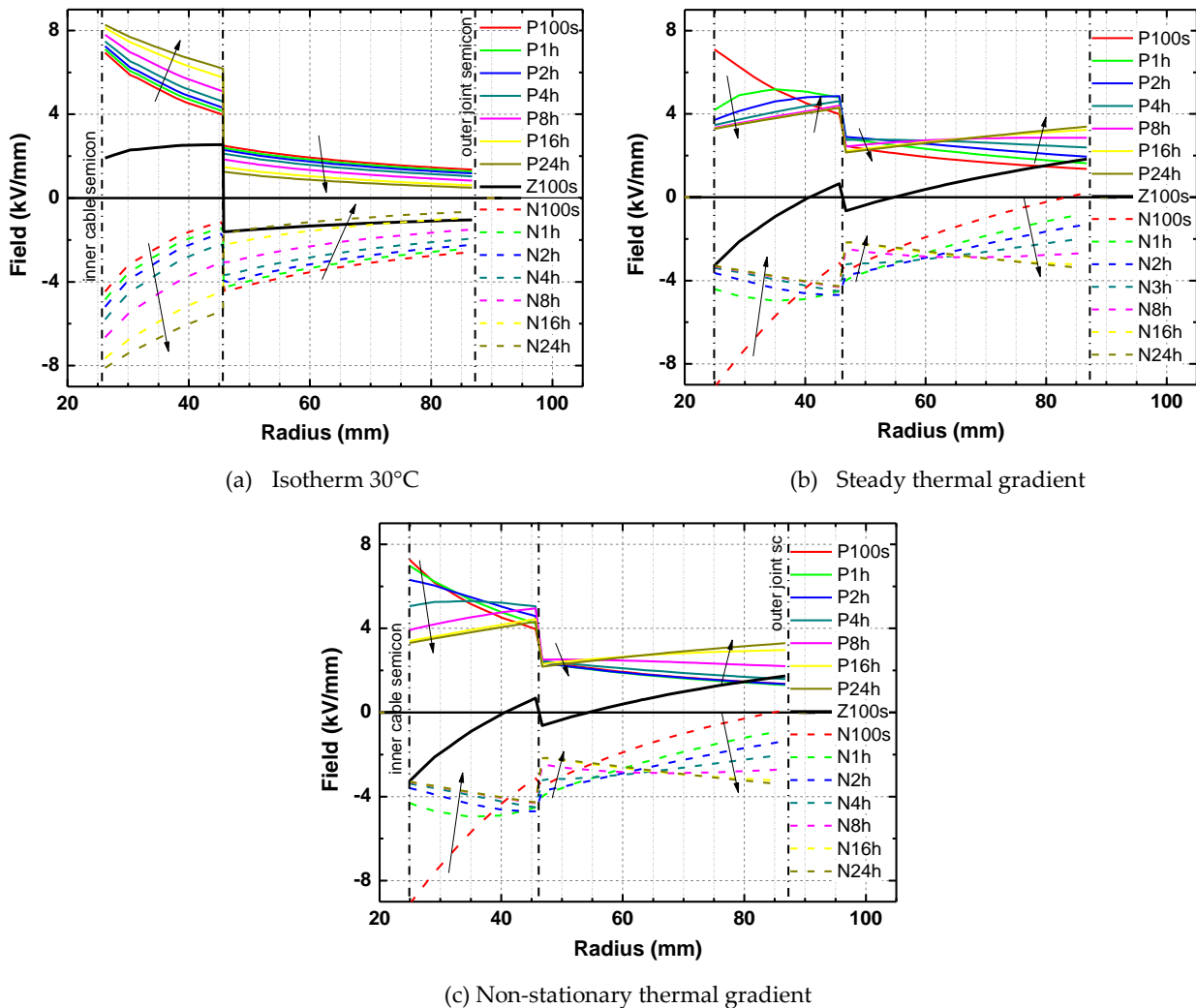


Figure 6. Radial field distribution in the XLPE/EPDM joint at different times after voltage application (+200 kV followed by polarity inversion) for different thermal conditions. Distribution taken at $z = 800$ mm, cf. Figure 3. Vertical lines indicate the boundaries of the insulators. The bold black curve corresponds to the reset to 0 V after 24 h at +200 kV. In the legend, P stands for positive voltage; N for negative. The arrows provide a guide to the eyes for the variation of the field as a function of time.

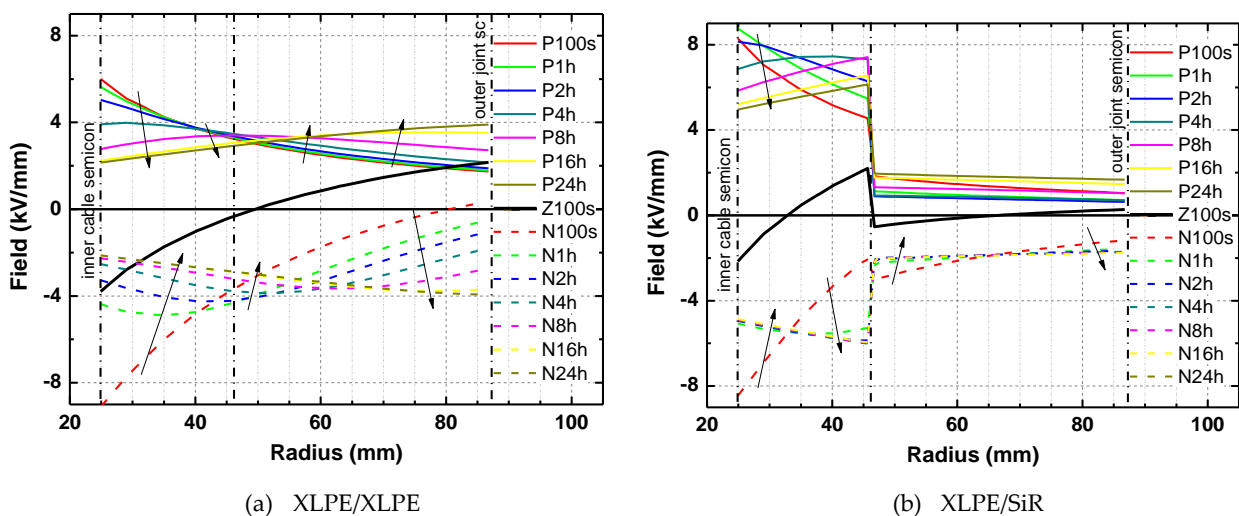
Under the conditions of a stationary thermal gradient, the electric field rapidly evolves towards a situation of equilibrium; one can consider that after 8 h this equilibrium is almost reached, cf. Figure 6b. Here within each of the materials the field tends to increase with the radius at long stressing time: this is because the thermal gradient produces a conductivity gradient whose effects exceed the variation of the field due to the cylindrical geometry. The residual field, taken 100 s after resetting the potential to zero, presents a profile different from that of the isothermal case. This residual field corresponds to the distortion introduced under DC stressing as compared to the geometric field distribution. The lower value of the residual field near the XLPE/EPDM interface results from the fact that with a temperature at the dielectric / dielectric interface of 45 °C, and fields of the order of 3 kV/mm, the conductivities of the two materials are quite close. In addition, the comparison of the field jumps for voltage on and voltage off conditions reveals a decrease within 100 s after setting the potential to zero, due to the partial dissipation of the interface charge. With the reversal of polarity, the field near the conductor is strongly reinforced.

The combination of unsteady electrical and thermal conditions, Figure 6c, mainly produces a slower kinetics towards the steady state compared to Figure 6b. Indeed, the temperature is initially lower,

251 and so is the dielectric time constant ($\tau = \epsilon / \sigma$ with a combination of physical quantities and geometry
 252 for the two materials) while the temperature gradient is setting up. The field distribution after 24 h is
 253 identical to that in the case of the stabilized gradient. A fortiori, it is the same for the following profiles.

254 The field profiles obtained for XLPE/XLPE and XLPE/SiR joints under non-stationary electrical and
 255 thermal conditions are presented in Figure 7. The field profiles for XLPE/XLPE joint are not very dif-
 256 ferent from the ones obtained in the case of XLPE/EPDM joint (Figure 7a vs. Figure 6c), except for the
 257 field step at the interface that has disappeared, due to permittivity effects. In the steady state situation,
 258 there is full stress inversion along the radius, i.e. a larger field at the outer diameter compared to inner
 259 diameter, as expected for a cable under thermal gradient [15].

260



261 **Figure 7.** Radial field distribution at different times after voltage application for a) XLPE/XLPE joint and
 262 b) XLPE/SiR joint under non-stationary thermal gradient. Same conventions as in Figure 6.

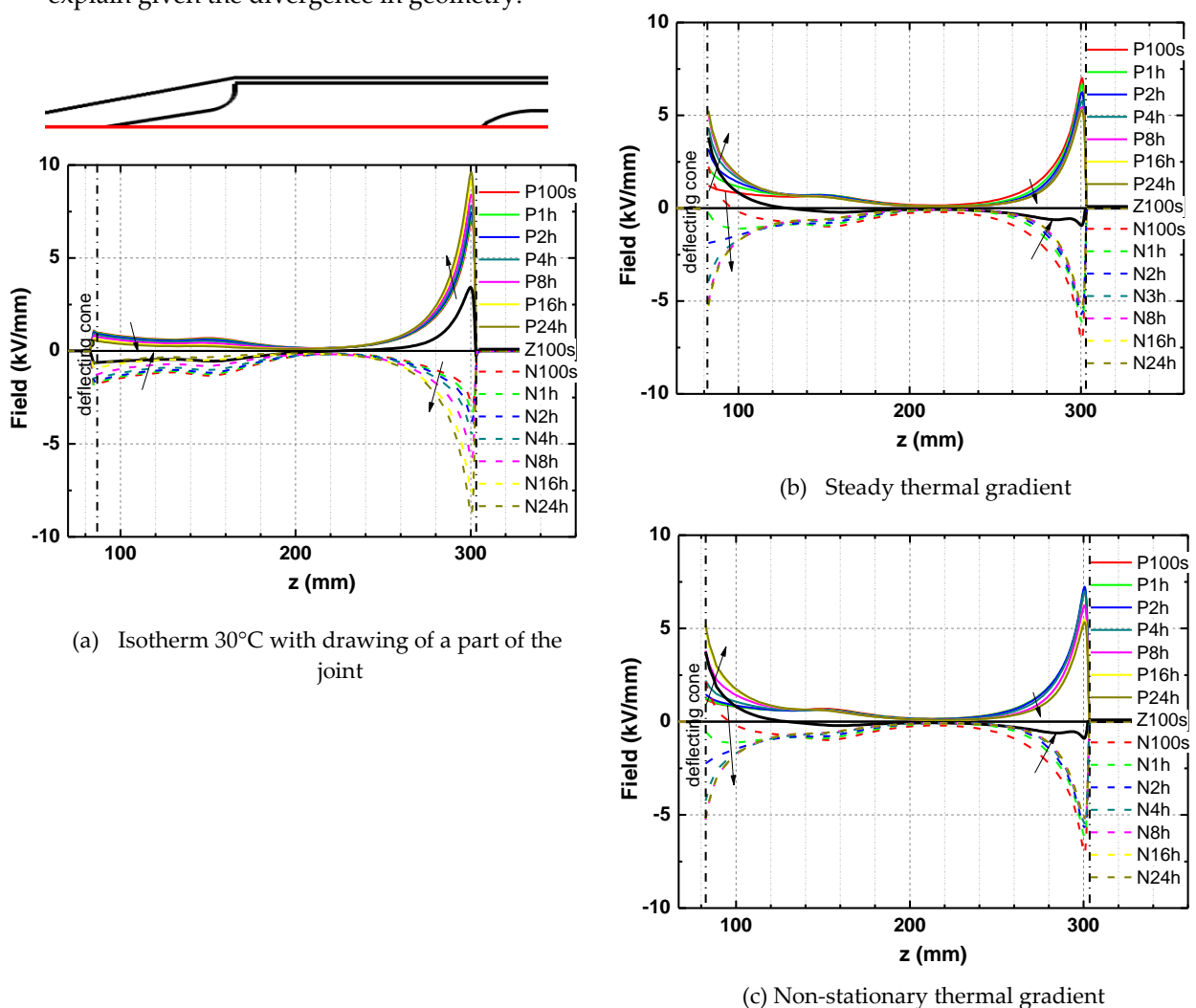
263 For the case of a SiR/XLPE joint (Figure 7b), the initial field step is quite large due to the high permi-
 264 tivity of SiR. In addition, when comparing the field at the dielectric/dielectric interface after 24 h and
 265 during the short-circuit, it can be seen that the field step is decreased within 100 s after resetting the
 266 potential, due to the partial dissipation of the interface charge. When the polarity is reversed, the field
 267 at the core is strongly reinforced. Here, the conductivity is higher in the SiR and therefore the field is
 268 higher in the XLPE part. The field redistribution is particularly fast after polarity inversion because of
 269 the high temperature in XLPE and high conductivity in SiR.

270

271 3.2.2. Tangential field distribution

272 The field distribution in the radial direction of the insulator can be relatively well anticipated and
 273 understood with knowledge of the behaviour of the materials. However, special attention should also
 274 be paid to the tangential electric field along the interface between the joint body and the cable under
 275 different electrical and thermal stresses. In fact, manufacturing the joint is a delicate step in which any
 276 imperfection such as a lack of adhesion or the presence of air bubble can be detrimental, even more if
 277 the electrical stress is significant. It has been reported that the tangential field at the interface of the
 278 two insulators is distributed with a strong non-uniformity, the field being strengthened in the insula-
 279 tor at the vicinity of the semiconductor connected to the ground [1, 8, 9, 10]. For these reasons, solu-
 280 tions with field-grading materials (FGM) [20] with strong non-linear properties have been adopted by
 281 some cable manufacturers [7]. However, this is not the rule, as reliability problems have arisen with
 282 this technology.

283 Figure 8 represents the tangential field profiles in the joint material (i.e. EPDM), near the interface
 284 between XLPE and EPDM (see arrow n°2 in Figure 3), as a function of time under stress, for the different
 285 thermal conditions previously explored. The tangential field values are the same in XLPE near
 286 the interface since the continuity rule imposes a continuity in tangential electric fields. Under isothermal
 287 conditions (Figure 8a), it is clear that the tangential field is significantly greater on the right of the
 288 figure, corresponding to the deflector region. This can be explained by a geometry that does not include
 289 a field-grading cone, unlike the potential reference side of the joint. In fact, some designs use a
 290 deflector cone also for the central part of the joint set to HV [9]. The quasi-constant axial field on the
 291 ground side corresponds precisely to the region ($z = 20\text{-}160\text{ mm}$) where the cone produces a non-radial
 292 component to the field. Over time, the tangential field tends to decrease on the ground side and to
 293 strengthen significantly on the HV side. These trends reflect the non-linear nature of the conductivity
 294 as well as the conductivity gradient due to the presence of two insulators. It is difficult to anticipate /
 295 explain given the divergence in geometry.

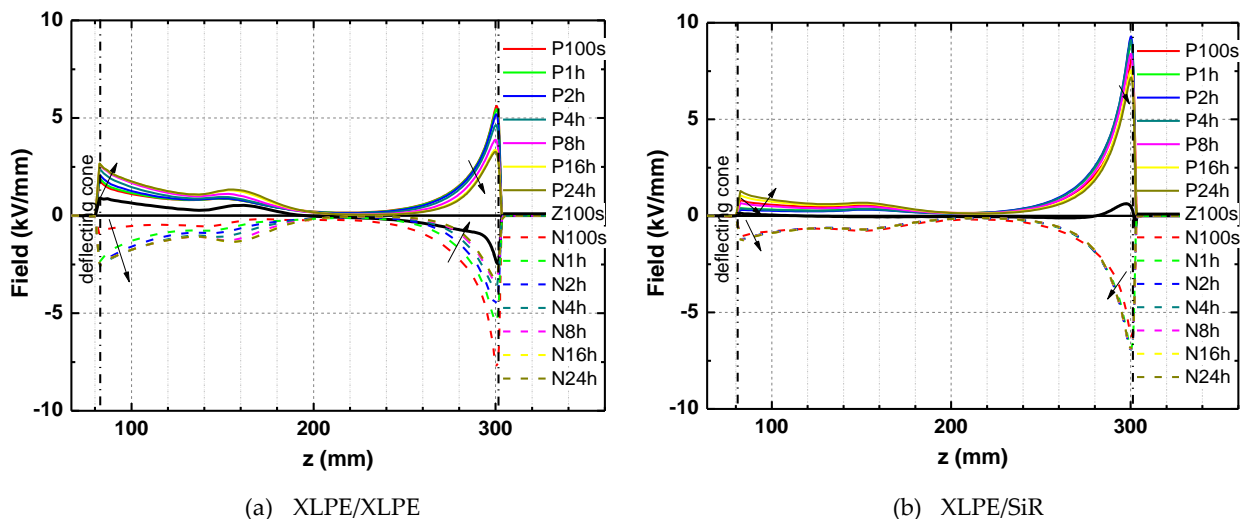


296 **Figure 8.** Tangential field distributions at the XLPE/EPDM interface at different times after voltage application.
 297 The drawing at the top of (a) represents a part of the joint. The axial field profiles are taken along the red line at
 298 the interface between XLPE and EPDM. Vertical lines define insulator boundaries. The curve in black corre-
 299 sponds to the reset to 0 after 24 h at +200 kV. Ground on the left; HV on the right. Same conventions as in Figure
 300 6.

301 Under thermal gradient condition (Figure 8b), the field increases with time on the cone side, by a factor
 302 3. As a result, in the first moments of the polarity reversal, the sign of the field is not reversed in this
 303 zone. On the HV side, the field variations are milder. The presence of a negative residual field at

304 grounding is noticeable. It is added to the applied field after stress polarity inversion, thereby produc-
 305 ing an over-stress. In case of non-stationary thermal conditions, Figure 8c, only mild differences are
 306 observed compared to the case of steady gradient. Only a faster convergence to steady state appears
 307 without further field distortion. Globally, the maximum tangential fields remain lower than in the case
 308 of isothermal conditions. This is not necessarily an effect of the thermal gradient but of the fact that,
 309 taking into account the average applied stresses, the conductivity values of the two insulators become
 310 closer by heating the joint. They are identical at 60 °C for a field of 4 kV/mm, while at 30 °C the equiv-
 311 alence is obtained under a field of 15 kV/mm (Figure 2) which is never reached here.

312 Using a single material, XLPE (Figure 9a), under non-stationary thermal and electrical conditions, the
 313 evolution of the field distribution is similar to the XLPE/EPDM one in the same conditions (Figure 8c).
 314 It means that, for the cases considered here, the temperature conditions are more important than the
 315 material nature. With the SiR joint material (Figure 9b) having a much larger conductivity than XLPE,
 316 there is practically no field distortion on the ground side (the residual field at voltage removal is nearly
 317 zero) and the field is small compared to the other cases. On the HV side, there is also a mild variation
 318 of the field with time, and hence weak residual field at grounding. Here the field reaches the highest
 319 values at about 7.5 kV/mm in steady state. The profiles are in fact similar to the ones of Figure 8a: the
 320 common feature here is a higher conductivity in the joint material than in XLPE.



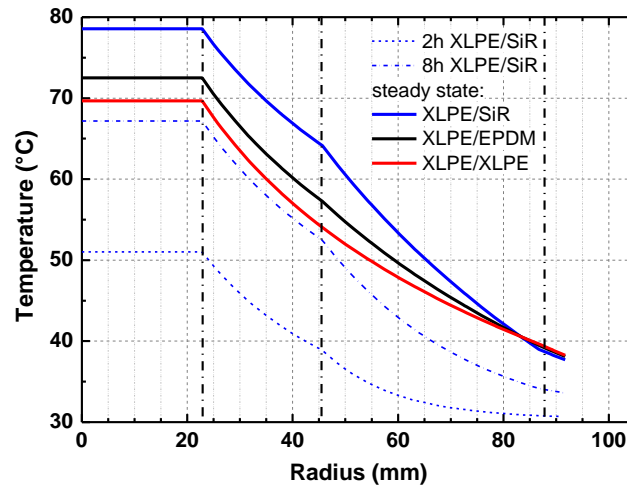
321 **Figure 9.** Tangential field distribution at a) XLPE/XLPE and b) XLPE/SiR interface at different times after voltage
 322 and current application (non-stationary electrical and thermal conditions). Vertical lines define insulator bound-
 323 aries. Same conventions as in Figure 6.

324

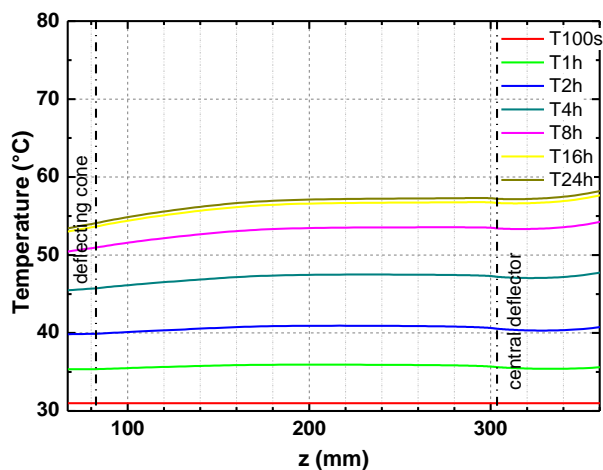
325 4. Discussion

326 Besides differences in the field dependence of conductivity between materials, the temperature distri-
 327 bution may affect the field distribution. Figure 10a represents the temperature distribution in the radial
 328 direction in quasi steady state for the three couples of materials considered. It shows that due to
 329 lower thermal conductivity in SiR, the temperature is significantly higher in the joint in this case. The
 330 temperature gradient is about 30°C with pure XLPE and it increases to 38°C in XLPE/SiR joint. At the
 331 dielectric/dielectric interface, the temperature is about 10°C higher in case of XLPE/SiR joint. This is a
 332 direct consequence of a lower thermal conductivity. This higher temperature in the insulation explains
 333 why the radial field redistributes faster in XLPE in Figure 7b than in Figure 6c for example once the
 334 thermal equilibrium is reached (negative polarity) since conductivity in XLPE increases by roughly a
 335 factor 3 in 10°C temperature variation considering the activation energy of 1 eV.

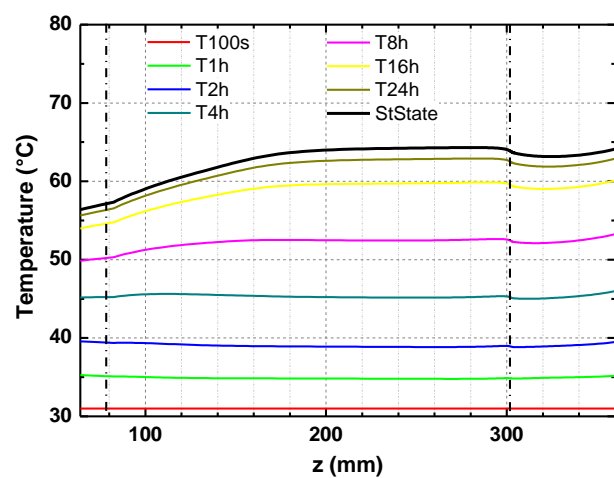
336 This substantially higher temperature with a SiR joint material compared to EPDM is reflected in Fig-
 337 ures 10b and 10c where the temperature variation along the interface is represented. Thermal gradi-
 338 ents along the axial direction are milder than under radial direction: the rise is by less than 10°C over
 339 a distance of ≈ 100 mm from the colder part, under the cone, to the central region. On the cone side, the
 340 temperature gradient is clearly larger with SiR than with EPDM joint material. On the deflector side,
 341 there is nearly no temperature variation along the z-axis.



(a) Radial temperature distribution



(b) XLPE/EPDM interface



(c) XLPE/SiR interface

342 **Figure 10.** a) Temperature profiles along the radial direction in quasi-steady state (24 h) for the considered three
 343 couples of materials and profiles during thermal transient for XLPE/SiR at 2 h and 8 h.
 344 (b, c): Temperature distributions along the interface, for XLPE/EPDM and XLPE/SiR joints at different times. In
 345 all cases, 1 kA is injected to the conductor and the initial temperature is 30 °C.

346

347 Above considerations show that the thermal properties of the joint material may significantly affect
 348 the temperature distribution in this joint design, and therefore, contribute to the actual field distribu-
 349 tion. Managing large temperature changes will go with more difficulty in optimising designs and se-
 350 lecting materials. Questions to discuss are on the expected joint material properties to get an optimum
 351 field distribution. At least three features are to be considered as criteria on the field for optimizing
 352 both design and materials:

-get a minimum capacitive field strength: this aspect concerns the field distribution short after DC voltage application, and, as importantly, field distributions in transient situations such as with over-voltages. In this case, the permittivity, and the geometric design, drive the field;

-get a minimum steady state DC field, notably the tangential part of the electric field;

-get a minimum field redistribution at polarity reversal, meaning that the residual field at grounding should be minimum, which implies that the capacitive and resistive field distributions are close.

The chosen design permits to appreciate, besides temperature effects and material effects, the dependence of field strengthening on geometrical features, with the cases of acute and obtuse angles respectively for the cone side and the deflector side, at the contact between the semicon and the joint materials.

On the cone side, the tangential field at short time is lowest for the case of SiR joint material, Figure 9b. The effect is purely associated to the value of permittivity, which is higher in the SiR. The highest field values (5 kV/mm) are obtained with EPDM under thermal gradient, cf. Figures 8b and 8c, whereas for the isothermal case at 30 °C, Figure 8a, the field remains low. All these results tend to show that the tangential electrical field is lower when the conditions are such that the field is moved to the cable (XLPE) insulation, either because of higher permittivity or high conductivity in the joint material: moved to a region of lower divergence, the field stays more concentrated in the radial direction. In order to confirm this, we have plotted in Figure 11 the tangential field for an isotherm at 70 °C with EPDM joint material. At this temperature, the electrical conductivity is lower in the EPDM than in XLPE. Here the tangential field under the cone is clearly enhanced compared to the case at 30 °C. With SiR joint material, large contrast in conductivities appears whatever the temperature and electric field values. The same happens also for EPDM at 30 °C, which explains the low intensity of the tangential field. For EPDM joint under thermal gradient, high fields are obtained at the tip of the cone (Figures 8b and 8c). This feature is presumably due to the thermal gradient that tends to move the field in this colder region.

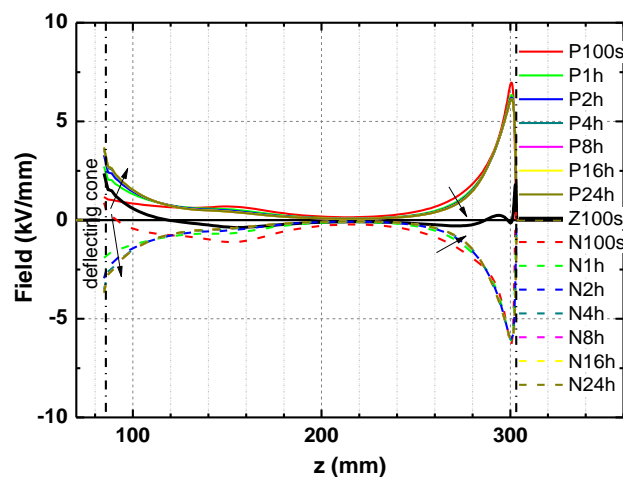


Figure 11. Tangential field distribution at XLPE/EPDM interface under isotherm condition at 70 °C.

The circulation of the field being conservative, it can be stated that:

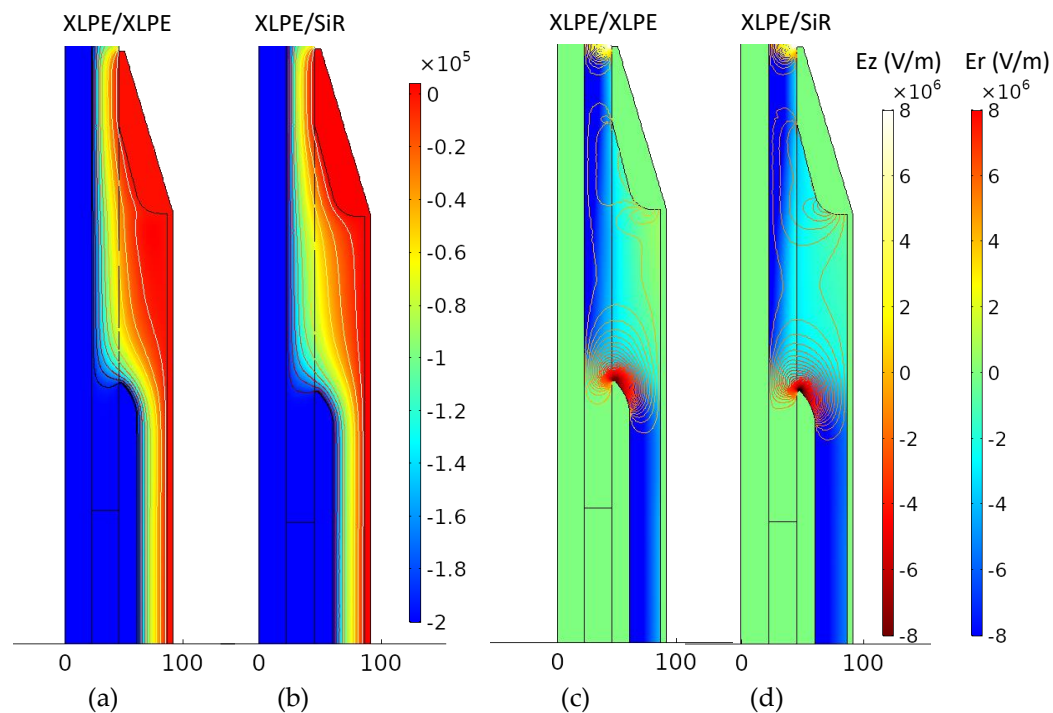
$$\int_c^d E_z dz = V_c - V_d \quad (5)$$

where c represents the deflecting cone and d the central deflector. Therefore, a field strengthening somewhere along the interface is compensated elsewhere along the interface, and the integral under

384 the tangential field component should be zero during the grounding step. Based on this rule, the tan-
 385 gential field near the central deflector would be the largest in case of SiR joint material and for the
 386 EPDM at 30 °C, i.e. in cases where a minimization of the tangential field under the cone is obtained. A
 387 better control of the field at the central deflector would be reached with shaping it as is done for the
 388 cone [4, 9].

389 According to Figure 2, XLPE is the most 'non-linear' material. XLPE joint material obviously gives
 390 perfect match of the conductivities and permittivities of the two insulations. Referring to Figure 9a, it
 391 can be considered that it corresponds to the case where the tangential field is the most homogeneously
 392 distributed. However, one main notice that the residual field near the central deflector is negative after
 393 positive voltage application. As a result, the field is strengthened after polarity reversal, which may
 394 represent a threat.

395 Figure 12 shows results for the potential and for the radial and tangential field distributions using
 396 different representations obtained with XLPE and with SiR joint materials just after polarity inversion.
 397 The tangential field around the central deflector is slightly higher in case of XLPE joint material. In
 398 both cases, it is quite low under the cone. Considering the potential or radial field maps, it is clear that
 399 the stress is more homogeneously distributed in case of SiR joint material. This behaviour results from
 400 the residual field set-up at the end of the previously applied positive voltage. After 24 h under stress,
 401 Figure 13, the situation has clearly evolved: the axial field under the cone has substantially increased
 402 for the XLPE joint, the radial field is more homogeneous, and the potential variations become
 403 smoother in this case.



404
 405

406 **Figure 12.** Potential distribution 3' after polarity reversal to -200 kV for (a) XLPE/XLPE and (b) XLPE/SiR joints.
 407 Corresponding radial (surface) and tangential (contour lines) field distributions
 408 for (c) XLPE/XLPE and (d) XLPE/SiR joints.

409

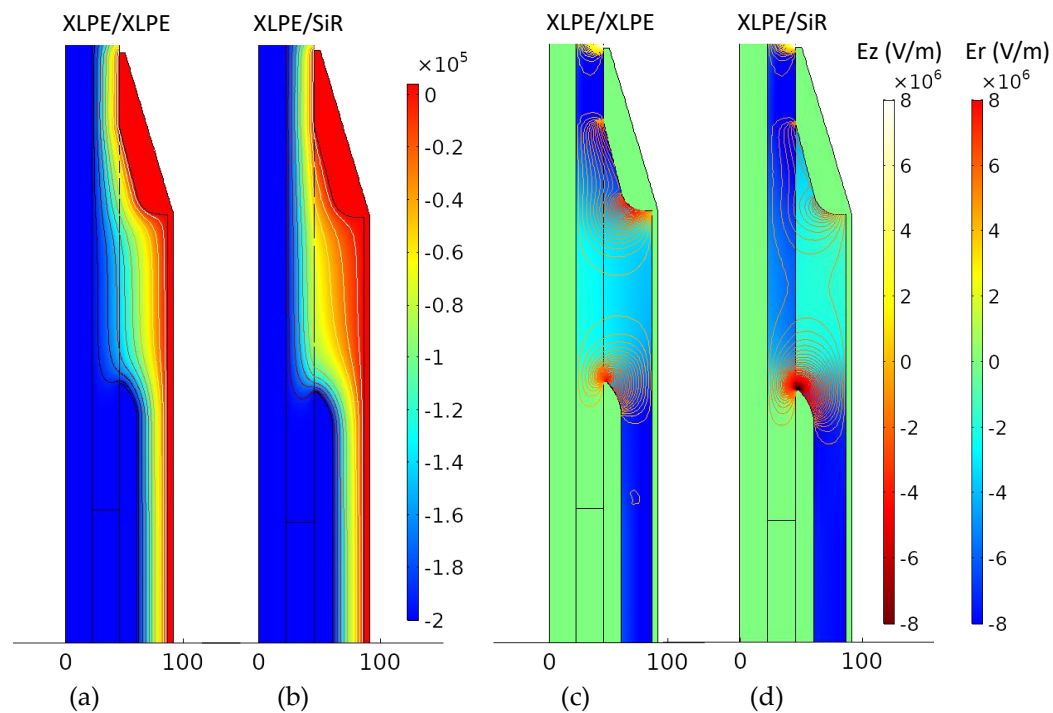


Figure 13. Potential distribution after 24h under -200 kV for (a) XLPE/XLPE and (b) XLPE/SiR joints. Corresponding radial (surface) and tangential (contour lines) field distributions for (c) XLPE/XLPE and (d) XLPE/SiR joints.

To obtain an equilibrated tangential field distribution along the interface, targeting continuity in the conductivities of the two insulations seems to be a good option. However, the field is not homogeneous in the joint, neither is the temperature and experimental data reveal that only in particular combinations (field-temperature), equal values of conductivity are obtained. It is in fact difficult to have similar conductivities from materials so different as silicones or EPDM and XLPE. The use of an elastomer remains essential to apply a homogeneous pressure and to match the shape of the insulated cable. This avoids surface tracking, surface discharges and the resulting failures. The design and modelling of joints on the standpoint of mechanical aspects was addressed recently by Lu *et al* [21]. However, the switch from XLPE to an elastomer leads to different dielectric behaviours, whether it be the conduction processes or the field and temperature dependencies, which result therefrom. Further, it is complicated to produce materials having a predefined electrical conductivity.

Besides continuity in electrical conductivity, the shape of deflecting pieces, the compatibility with the capacitive field distribution and the possibility of having resistive field grading are worth considering. The resistive field grading, since it is with slow reaction, does not solve the problem of transient stresses obtained during operation such as polarity reversal or during lightning impulse [14]. A target for materials resistivity could be to reach the same field redistribution as obtained in the ac case with the capacitive distribution. An immediate consequence is that the residual field at grounding would be minimum. As regards the field grading due to field dependence of conductivity, it is not easy to control here as the average fields are relatively low, of the order of 5 kV/mm, and in general for insulating materials, the threshold for non-linearity is not much lower. Resistive field grading materials have comparatively lower threshold fields, typically 1 kV/mm. An advantage of FGM layer is to decouple the stresses in the insulation material of the cable and the joint body effectively. The design remains a tactful exercise, with trade-off to be done between losses, fields, and operating temperature [22]. Finally, an important point is the thermal characteristics of the materials. In the examples shown

here, the insulation under the cone tends to be colder than the body of the joint, meaning that a counter-effect of field grading is obtained, i.e. field enhancement in the cold parts. Therefore, improvement could be brought by implementing joint material with higher thermal conductivity.

Compared to other studies on field distributions in joints, the work presented here considers the transient conditions of field establishment whereas very often only a direct resolution in stationary state is proposed. Multiple stress conditions can be tested. This is quite easily achievable, but it is important to stress that the collection of experimental data on conductivity, representative of materials in their operating environment, is a major preliminary step in all these modelling and design tasks.

5. Conclusions

The field distribution in HVDC cable joints has been investigated in non-stationary electrical and thermal conditions, considering XLPE as cable insulation and different materials as insulation joint: EPDM, XLPE and SiR. The joint materials differed by their field and temperature dependencies of electrical conductivity and by their thermal conductivity. The radial distribution of the field follows predictable trends with temperature, either in isothermal or thermal gradient conditions, depending on materials electrical conductivity. The temperature gradient, and the nonlinear conduction, play a role of field grading. However, this effect is annihilated after polarity reversals: a transient overstress appears just after voltage polarity inversion in all cases involving a thermal gradient.

The tangential distributions of the field along the interface between the insulator of the joint and that of the cable have temporal and temperature behaviours that are not deduced in a simple way from the stress conditions. Under the deflecting cone, the smallest field values and mildest field redistribution are obtained with the joint insulation having the highest electrical conductivity (SiR). This feature has been explained by a shift of the field towards the cable insulation in which the geometrical features of the system produce less axial component. At the level of the high voltage semicon (central deflector), it is clear that the tangential field is higher when the mismatch between the conductivity of the two insulations is larger. In addition, the field grows as a function of time under stress. This is verified whether the system is in isothermal or thermal gradient conditions. Thermal gradient effects are still to be analysed.

The thermal conductivity of the joint material has a substantial impact on the temperature in the core of the joint and at the interface. This temperature gradient is obvious along the radial direction and is effective along the axial direction too. The joint being cooler under the deflecting cone, field strengthening appears in this region.

Author Contributions: “Conceptualization, G.T.; experiments, simulation, T.T.N.V.; validation, formal analysis, T.T.N.V., G.T. and S.L.R.; writing—original draft preparation, T.T.N.V., G.T.; reviewing, S.L.R. All authors have read and agreed to the published version of the manuscript.”

Funding: This work is supported by CNRS International Scientific Cooperation Program (PICS) N° PICS07965.

Data Availability Statement: Experimental data on conductivity are more completely described in [12]. Specific simulation data can be available upon request to the corresponding authors.

Conflicts of Interest: The authors declare no conflict of interest.

References

1. Mazzanti, G.; et al. The insulation of HVDC extruded cable system joints. Part 1: Review of materials, design and testing procedures. *IEEE Trans. Dielectr. Electr. Insul.* **2019**, *26*, 964-972
2. Ye, H.; Fechner, T.; Lei, X.; Luo, Y.; Zhou, M.; Han, Z.; Wang, H.; Zhuang, Q.; Xu, R.; Li, D. Review on HVDC cable terminations. *IET High Volt.* **2018**, *3*, 79-89
3. Jörgens, C.; Clemens, M. A review about the modeling and simulation of electro-quasistatic fields in HVDC cable systems. *Energies* **2020**, *13*, 5189
4. Frobin, S.J.; Niedik, C.F.; Freye, C.; Jenau, F.; Häring, D.; Schröder, G. A generic approach for HVDC cable accessories modelling. Proc. 2018 IEEE Internat. Conference on Dielectrics (ICD), Budapest, Hungary, July 2018, IEEE, pp. 1-6.
5. Albertini, M.; Cotugno, S.; Pietribiasi, D.; Remy, C. HPTE Extruded cables polarity reversals performance in LCC HVDC systems," Proc. 2020 AEIT International Annual Conference (AEIT), Catania, Italy, Sept. 2020, pp. 1-6, doi: 10.23919/AEIT50178.2020.9241205.
6. Saltzer, M.; Christen, T.; Sörqvist, T.; Jeroense, M.J.P. Electrothermal simulations of HVDC cable joints. Proc 2011 VDE-ETG Workshop Feldsteuernde Isoliersysteme - ETG-Fachbericht 131, Darmstadt, Germany, Nov. 2011, pp. 1-6
7. Fälth, F.; Kumar, S.; Ghorbani, H. Robustness analysis of classical high voltage joint design under high voltage DC stress", Proc. 23rd Nordic Insulation Symposium, Trondheim, Norway, June 2013, pp. 140-145
8. Ghorbani, H.; Jeroense, M.; Olsson, C.-O.; Saltzer, M. HVDC cable systems—Highlighting extruded technology. *IEEE Trans. Power Deliv.* **2014**, *29*, 414-421
9. Ye, H.; Han, Z.; Luo, Y.; Zhuang, Q.; Fechner, T.; Wang, H.; Lei, X. Design aspects on HVDC cable joints. Proc. 12th IEEE Internat. Conf. Properties and Applications of Dielectric Materials (ICPADM), Xi'an, China, May 2018, IEEE, pp. 300-304
10. Mauseth, F.; Haugdal, H. Electric field simulations of high voltage DC extruded cable systems. *IEEE Electr. Insul. Mag.* **2017**, *33_4*, 16-21
11. Stancu, C.; Notingher, P.V.; Notingher, P.; Lungulescu, M. Space charge and electric field in thermally aged multilayer joints model. *IEEE Trans. Dielectr. Electr. Insul.* **2016**, *23*, 633-644
12. Vu, T.T.N.; Teyssedre, G.; Vissouvanadin, B.; Le Roy, S.; Laurent, C. Correlating conductivity and space charge measurements in multi-dielectrics under various electrical and thermal stresses. *IEEE Trans. Dielectr. Electr. Insul.* **2015**, *22*, 117-127
13. Vu, T.T.N.; Teyssedre, G.; Vissouvanadin, B.; Le Roy, S.; Laurent, C.; Mammeri, M.; Denizet, I. Field distribution under temperature gradient in polymeric MV-HVDC model cable: simulation and space charge measurements. *Eur J. Electr. Engg.* **2014**, *17*, 307-325
14. Baferani, M. A.; Shahsavarian, T.; Li, C.; Tefferi, M.; Jovanovic, I.; Cao, Y. Electric field tailoring in HVDC cable joints utilizing electro-thermal simulation: effect of field grading materials. Proc. 2020 IEEE Electrical Insulation Conference (EIC), Virtual, June 2020, IEEE, pp. 400-404
15. Boggs, S.; Dwight, H.; Hjerrild, J.; Holbol, J.T.; Henriksen, M. Effect of insulation properties on the field grading of solid dielectric DC cable. *IEEE Trans. Power Deliv.* **2001**, *16*, 456-462
16. Li, Z.Y.; Sun, W.F.; Zhao, H. Significantly Improved electrical properties of photo-initiated auxiliary crosslinking EPDM used for cable termination. *Polymers* **2019**, *11*, 2083
17. Li, D.; Zhu, Z.; Yang, L.M.; Ma, Y.L. Research on nonlinear EPDM for ±525kV HVDC cable accessories. *MATEC Web of Conferences* **2019**, *260*, 02001 <https://doi.org/10.1051/mateconf/201926002001>
18. Qin, Y.J.; Shang, N.Q.; Chi, M.H.; Wang, X.Y. Impacts of temperature on the distribution of electric-field in HVDC cable joint. Proc. 2015 IEEE Internat. Conf. Properties and Applications of Dielectric Materials (ICPADM), Sidney, Australia, Sept. 2015, IEEE, pp. 224-227
19. Vu, T.T.N.; Teyssedre, G.; Le Roy, S.; Laurent, C. Maxwell-Wagner effect in multi-layered dielectrics: interfacial charge measurement and modelling. *Technologies* **2017**, *5*, 27
20. Donzel, L.; Greuter, F.; Christen, T. Nonlinear resistive electric field grading Part 2: Materials and applications. *IEEE Electr. Insul. Mag.* **2011**, *27_2*, 18-29
21. Luo, Y.; Han, Z.; Zhou, M.; Wang, H. A Sophisticated method of the mechanical design of cable accessories focusing on interface contact pressure. *Energies* **2020**, *13*, 2976
22. Späck-Leigsnering, Y.; Ruppert, M. G.; Gjonaj, E.; De Gersem, H.; Koch, M. Towards electrothermal optimization of a HVDC cable joint based on field simulation. *Energies* **2021**, *14*, 2848